nature communications

Article

https://doi.org/10.1038/s41467-025-61621-4

Tumor vessel-adaptable adhesive and absorbable microspheres for sustainable transarterial chemoembolization therapy

Received: 3 January 2025

Accepted: 26 June 2025

Published online: 07 July 2025

Check for updates

Jiakun Guo[1,3], Jintao Huang[2,3], Zuliang Huang[1], Di Hu[2], Hujing Tan[1], Yan Wang[1], Chao Deng[1] ✉, Xiaoli Zhu[2] ✉ & Zhiyuan Zhong[1] ✉

Transarterial chemoembolization (TACE) is a common clinical intervention used for unresectable liver tumors, but conventional embolic microspheres generally exhibit slack vascular stacking and suboptimal drug release. Here, we report tumor vessel-adaptable, adhesive, and absorbable microspheres (3Asphere) based on hyaluronic acid developed using microfluidic and radical polymerization techniques for sustained TACE therapy of liver tumors. 3Asphere presents uniform sizes, gradual degradation over two months, and fast encapsulation and sustained release of chemotherapeutics such as epirubicin, irinotecan, and cisplatin. Interestingly, 3Asphere with high elasticity enables robust vascular embolization, effectively blocking rabbit renal blood supply for over one month. In rabbit VX2 orthotopic liver tumors, 3Asphere actively binds to endothelial cells via CD44 and inhibits tumor growth, affording significant survival benefits compared to commercial Embosphere®. TACE with epirubicin-loaded 3Asphere further enhances tumor inhibition and prevents lung metastasis. 3Asphere provides a versatile and advanced TACE therapy that might alleviate liver tumors.

Transarterial chemoembolization (TACE), a minimally invasive interventional therapeutic strategy, is considered the first-line therapy for intermediate B-stage hepatocellular carcinoma (HCC) and involves injecting embolic agents into the target blood-supplying artery to synergistically induce tumor arterial embolization and localized chemotherapy[1–3]. Several embolic microspheres with easy handling, predictable shape, and calibrated sizes, including CalliSpheres®, DC Bead®, and HepaSphere®, have been approved for TACE therapy[4,5]. However, the therapeutic outcomes are significantly compromised by unmanageable drug release and insufficient embolization due to the slack and passive stacking of embolic agents in complex vascular systems[6–9]. The mechanical properties of embolic microspheres, particularly their viscoelastic deformation capacity and vessel-adaptability to reach arterial branches in liver tumors, are critical not only for efficient embolization but also for reducing procedural complications[10,11]. Recently, lipiodol microspheres stabilized by Janus particles or amphiphilic polyurethane have been reported to exhibit decent viscoelastic deformation capacities for close packing and compact embolization of vessels down to 40 μm, providing efficient ear and renal embolization in rabbits[11,12]. To accelerate drug loading and improve drug release, charged moieties (e.g., sulfonic acid, acrylic acid) and degradable components (e.g., polyester, polysaccharides, and gelatin) have been introduced into embolic microspheres[13–15].

Distinct from emulsion microspheres and stiff microparticles, covalently crosslinked and water-enriched microspheres offer the right balance of viscoelasticity for effective embolization and a robust structure that minimizes the risk of off-target vessel blockade.

[1]Biomedical Polymers Laboratory, and Jiangsu Key Laboratory of Advanced Functional Polymer Materials, College of Chemistry, Chemical Engineering and Materials Science, and State Key Laboratory of Radiation Medicine and Protection, Soochow University, Suzhou, China. [2]Department of Interventional Radiology, The First Affiliated Hospital of Soochow University, Suzhou, China. [3]These authors contributed equally: Jiakun Guo, Jintao Huang.
✉e-mail: cdeng@suda.edu.cn; zhuxiaoli90@163.com; zyzhong@suda.edu.cn

Meanwhile, polysaccharides with their inherent degradability and functionality can easily manage drug loading and release processes[16–20]. In this study, we develop vessel-adaptable, adhesive, and absorbable microspheres (3Asphere) based on hyaluronic acid (HA) using microfluidic and radical polymerization techniques for sustainable TACE therapy of liver tumors (Fig. 1). HA characterized by favorable biocompatibility and biodegradability can actively bind to CD44 overexpressed on tumor-associated vessels and tissues to promote microsphere adhesion to vessels. Different from turbulent agitation and uncontrolled hydrodynamic forces by conventional bulk emulsion polymerization, microfluidics enables precise fluid manipulation by leveraging laminar flow regime and geometric confinement within micron-scale channels, and provides droplets with a uniform size and good batch-to-batch reproducibility[21,22]. 3Asphere with precise sizes enabled by microfluidics and decent elasticity is expected to contribute to compact embolization of distal tumor vessels. Leveraging the multiple interactions and good biodegradability, 3Asphere allows quantitative encapsulation of epirubicin (EPI, up to 100 mg/mL) within 1 min as well as sustained and nearly complete drug release (>95% EPI) within 56 days. In rabbits bearing orthotopic VX2 tumors, transarterial embolization with 3Asphere effectively inhibits tumor growth, which is boosted by encapsulating thrombin, a naturally occurring protein hydrolase for biological hemostasis[23,24], through the formation of blood clots in distal and finer tumor vessels. TACE with EPI-loaded 3Asphere further enhances tumor inhibition and prevents lung metastasis.

Results

Tailored fabrication of 3Asphere

3Asphere was facilely fabricated by combining microfluidic and radical polymerization techniques under UV irradiation (Supplementary Fig. 1). The size-defined microdroplets were generated through rapid shearing of an aqueous solution of HA-2-aminoethyl methacrylate with mineral oil containing 9 wt.% Span 80 (Supplementary Movie 1) and then photocrosslinked to generate stable microspheres, as evidenced by the complete disappearance of methacrylate absorption at 1570 cm^{-1} in Fourier-transform infrared spectra (Supplementary Fig. 2). By adjusting the polymer concentration, chip depth, and flow rates of the aqueous and oil phases, the microsphere size could be precisely controlled in the range of 40–180 μm (Fig. 2a, b). 3Asphere presented defined sizes of 60, 90, and 150 μm, with a coefficient of variation (CV) value of less than 2.0%, when the chip depth was increased from 70 to 150 μm while the polymer concentration and flow rate ratios were fixed (Fig. 2c–e). Thus formed microspheres were designated 3Asphere-60, 3Asphere-90, and 3Asphere-150, respectively. In contrast, commercial Embosphere® and CalliSpheres® exhibited broad size distributions (40–120 and 100–300 μm, respectively) with CV values of 22.1% and 24.9%, respectively (Supplementary Fig. 3).

3Asphere revealed marked stability with negligible size changes after sterilization at 120 °C and long-term (>12 months) storage (Supplementary Figs. 4, 5), and steady suspension in an iodixanol solution for transcatheter administration (Supplementary Fig. 6). As HA can be degraded by endogenous hyaluronidase (HAase)[25,26], here

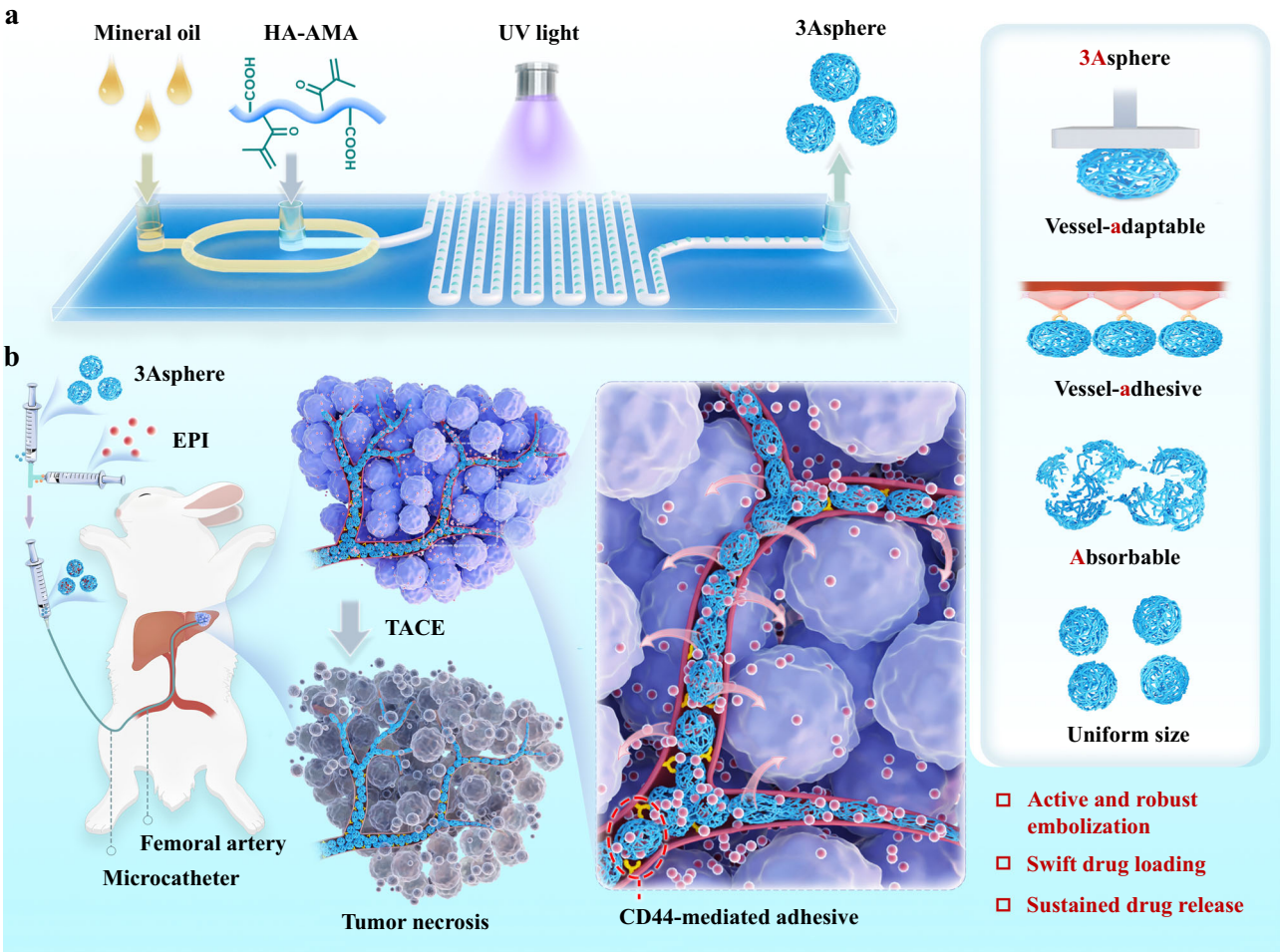

Fig. 1 | Schematic illustration of tumor vessel-adaptable, adhesive, and absorbable microspheres (3Asphere) for sustainable transarterial chemoembolization (TACE) therapy. a 3Asphere based on hyaluronic acid derivatives is constructed by combining microfluidic and radical polymerization techniques. **b** 3Asphere featured with efficient embolization, fast drug loading, and sustained drug release affords potent treatment of hepatocellular carcinoma (HCC).

https://doi.org/10.1038/s41467-025-61621-4

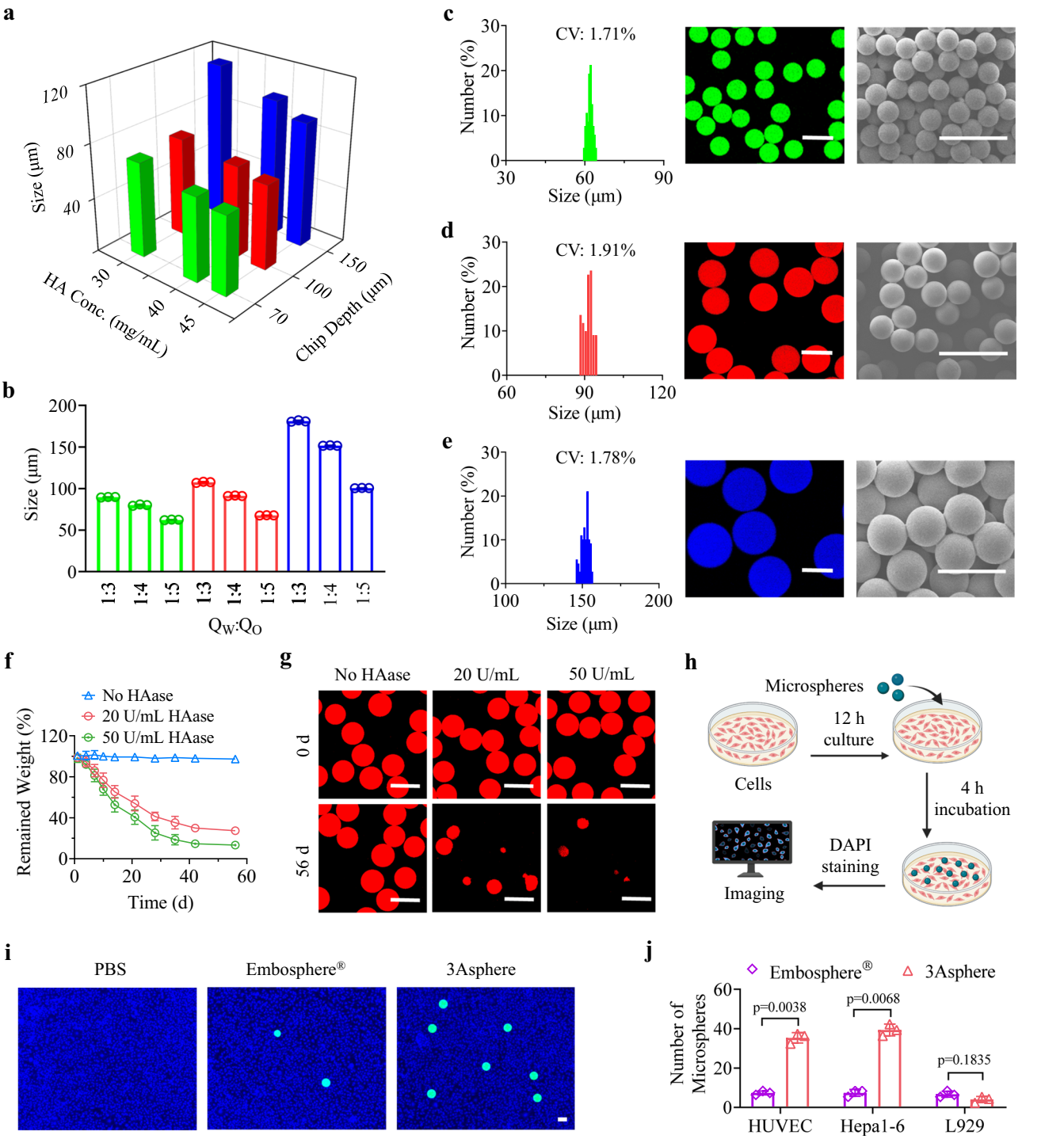

Fig. 2 | Construction and characterization of 3Asphere. a–e Size changes of 3Asphere with varying HA concentrations, chip depth, and flow rate ratios. **a** Mean size map controlled by adjusting HA concentrations and chip depth ($n = 3$ independent experiments). **b** Mean size controlled by adjusting the flow rate ratios of water and oil phases (Q_w: Q_o) ($n = 3$ biological samples). A chip depth of 70 μm (green), 100 μm (red), or 150 μm (blue) was used to prepare different 3Asphere. **c–e** Size distribution of 3Asphere with average diameters of 60 μm (**c**), 90 μm (**d**), and 150 μm (**e**) was calculated from microsphere images taken by inverted fluorescence microscope (left column), and 3Asphere morphology was observed by confocal laser scanning microscope (CLSM, middle column) and scanning electron microscope (SEM, right column) ($n = 3$ independent experiments). **f** Degradation profiles of 3Asphere at hyaluronidase (HAase) concentrations of 20 and 50 U/mL ($n = 3$ biological samples). **g** Morphology change of 3Asphere-90 in the presence of HAase observed by CLSM ($n = 3$ independent experiments). **h** Illustration of in vitro CD44-mediated binding experiment. Created in BioRender. BioRender.com/q8xzmwo. **i** Fluorescence microscopy images of Cy3-labeled 3Asphere-90 and Embosphere® bonded on HUVEC ($n = 3$ independent experiments). **j** Number of microspheres bonded on different cells ($n = 3$ biological samples). Statistical analysis was performed using unpaired two-tailed Student's t-test. All scale bars: 100 μm. Data are presented as mean ± SD. Source data are provided as a Source Data file.

we investigated the enzymatic degradation behavior of 3Asphere. In the presence of HAase (20 U/mL), 3Asphere tended to degrade over time, with approximately 35% of 3Asphere degrading within the first 2 weeks and the percentage of degradation increasing to 73% after 8 weeks (Fig. 2f). Elevating the HAase concentration to 50 U/mL accelerated degradation and enhanced morphological devastation (Fig. 2g). Following subcutaneous implantation in rats, 3Asphere exhibited a progressive degradation pattern, with approximately 17% degradation in the first week and more than 90% degradation after 8 weeks (Supplementary Fig. 7). The above results confirm that 3Asphere would undergo enzymatic degradation by endogenous HAase and is absorbable in vivo. In contrast, commercial Embosphere® is a collagen-coated acrylic microsphere in which the majority of the microsphere is acrylic polymer and hence not degradable. Hematoxylin and eosin (H&E) analysis showed that the mild inflammatory response induced by 3Asphere nearly vanished within 2 weeks (Supplementary Fig. 8). Cell lines (L929, Hepa1-6, SMMC-7721, HepG2, and VX2) incubated with 3Asphere for 48 h revealed over 95% cell viability (Supplementary Fig. 9), and erythrocytes treated with 3Asphere at concentrations of 0.2–1.0 mg/mL exhibited hemolysis rates below 1.0% (Supplementary Fig. 10), highlighting their decent biocompatibility and safety. Leveraging the HA-CD44 axis, 3Asphere demonstrated apparent binding to CD44-coated plates (Supplementary Fig. 11) and CD44-positive human umbilical vein endothelial cells (HUVEC) and Hepa1-6 HCC cells (Fig. 2h–j and Supplementary Fig. 12), suggesting potentially active adhesion of 3Asphere to the endothelial cells of tumor vessels. In comparison, commercial Embosphere® with collagen on the surface revealed limited binding to CD44-coated plates and CD44-positive cells.

Mechanical properties and embolization effect of 3Asphere

3Asphere revealed a low viscosity (20–1400 mPa•s) at varying shear rates, shear-thinning behavior (Fig. 3a), and low storage modulus (G′) of 90–100 Pa (Fig. 3b), benefiting the catheter and vessel delivery. In addition, 3Asphere like CalliSpheres® and Embosphere® displayed quasi-elastic characteristics during compression deformation (Fig. 3c). Under compression up to 50% strain, less compression force was needed for 3Asphere (ca. 0.8 N versus 1.4 and 1.8 N for CalliSpheres® and Embosphere®, respectively), indicating that 3Asphere is more subject to deformation. After 50% compression deformation for 20 s or transcatheter injection, 3Asphere maintained an integral structure and morphology without any fragmentation (Supplementary Figs. 13, 14), signifying the feasibility of transcatheter delivery.

Glass capillary tubes with one end sealed were utilized to simulate the embolization process. Following injection from the opposite end, 3Asphere-90 demonstrated tight aggregation with vessel-adaptable shapes including spheres, ellipsoids, dumbbells, strings, and furcation in the tube, whereas Embosphere® revealed relatively slack packing with a predominantly spherical shape (Fig. 3d, e). Moreover, 3Asphere presented a ratio of embolized volume (V_{em}) to theoretical volume (V_{th}) of 1.3, a void fraction of approximately 28%, and aspect ratios of 1.17 (Fig. 3f–h), corroborating that 3Asphere possesses superior viscoelasticity and stack ability for vascular embolization.

Rabbit renal arteries were utilized as a model to verify the in vivo embolic effect of 3Asphere. After slow injection of a mixture of 3Asphere-90 (3×10^5 spheres/mL, 1.0 mL) and iodixanol (1.0 mL) into the right renal artery using a 2.4-F microcatheter, digital subtraction angiography (DSA) clearly revealed that the arterial lumen of the right kidney was completely occluded, as indicated by the disappearance of the iodixanol signal in this kidney (Fig. 3i). The embolic effect was then monitored using computed tomography angiography after intravenous injection of iodixanol, and negligible signal was observed in the right kidney during 28 days after embolization (Fig. 3j), suggesting that no vessel recanalization occurred and long-term robust occlusion was achieved by 3Asphere. H&E staining revealed that 3Asphere gradually degraded over time (Supplementary Fig. 15), and induced obvious damage to the glomerular and tubular structures as well as tissue necrosis within the embolized right kidney (Fig. 3k).

Size effect on transarterial embolization

An orthotopic tumor model established by in situ injection of VX2 tumor blocks into the liver parenchyma of rabbits was employed to evaluate the size effect of 3Asphere on embolization therapy (Fig. 4a). DSA images displayed that 3Asphere of different sizes induced clear embolization with nearly vanished iodixanol signals at the tumor sites, following administration at the proper hepatic artery (PHA) via a 2.4-F microcatheter (Fig. 4b and Supplementary Fig. 16). Notably, 3Asphere inhibited VX2 tumor growth in a size-dependent manner, in which 3Asphere with smaller sizes afforded better tumor suppression (Fig. 4c, d). The therapeutic efficacy was further assessed using magnetic resonance imaging (MRI), including T1-weighted (T1), T2-weighted (T2), and Gd-DTPA enhanced T1 (T1+) imaging on days 0 and 14. The results corroborated that 3Asphere suppressed tumor growth in a size-dependent manner (Fig. 4e). Diffusion-weighted imaging (DWI) was used to assess tumor cell necrosis by measuring the microscopic mobility of free water molecules to determine the apparent diffusion coefficient (ADC)[27]. Following 14 days of embolization, the ADC values for treated VX2 tumors were in the following order: 3Asphere-60 > 3Asphere-90 > 3Asphere-150 ≈ Embosphere® (Fig. 4f), corroborating that smaller-sized microspheres caused more cell necrosis, which was further verified by H&E staining (Supplementary Fig. 17). Notably, rabbits treated with 3Asphere-90 revealed a significantly extended median survival time (MST) of 47 days, possibly owing to the less severe damage to healthy liver tissue (Fig. 4g). H&E staining analysis displayed that 3Asphere-90 caused no obvious inflammation and necrosis in the main organs (liver, lungs, kidneys, spleen, and heart) (Supplementary Fig. 18) and little change in body weight over 14 days (Fig. 4h). Serum concentrations of aspartate aminotransferase, alanine aminotransferase, creatinine, and urea in rabbits increased after embolization with 3Asphere-90 but rapidly returned to normal levels on day 7 (Supplementary Fig. 19), indicating negligible liver and kidney function impairment.

3Asphere distribution in the liver, tumors, and vessels following embolization

Cy5-labeled 3Asphere (Cy5-3Asphere) was employed to assess the microsphere distribution in the liver and tumors 3 days after embolization. Consistent with the size-dependent tumor suppression, 3Asphere with smaller sizes accumulated to higher levels in the tumors (Fig. 5a), in which 3Asphere-60 (45.4%) revealed over 1.3- and 4-fold higher tumor enrichment than 3Asphere-90 (33.3%) and 3Asphere-150 (10.7%), respectively (Fig. 5b). Compared with the negligible necrosis observed in normal liver tissue of rabbits treated with 3Asphere-90 and 3Asphere-150, obvious necrosis was presented in the 3Asphere-60 group (Fig. 5c), suggesting that small 60-μm microspheres might move into the distal vessels of the normal liver and cause necrosis. No microspheres were observed in other major organs (heart, spleen, lungs, and kidneys) after embolization with 3Asphere of different sizes (Supplementary Fig. 20), implying that off-target vessel blockade unlikely occured in major organs.

Histological analysis was employed to explore microsphere dispersal in the tumor vasculature. Following the embolization of VX2 tumors for 3 days, H&E images of tumor vessels revealed that the deformable shape of 3Asphere allowed them to adapt to blood vessels of different levels and penetrate distally for efficient embolization of fine vessels down to 20–60 μm (Fig. 5d). 3Asphere-60 and 3Asphere-90 were preferentially distributed in vessels 10–20 μm smaller than the microsphere size, whereas 3Asphere-150 was distributed sporadically in the tumor vessels (Fig. 5e, Supplementary Fig. 21). Embosphere® with higher stiffness predominantly presented a spherical morphology and

https://doi.org/10.1038/s41467-025-61621-4

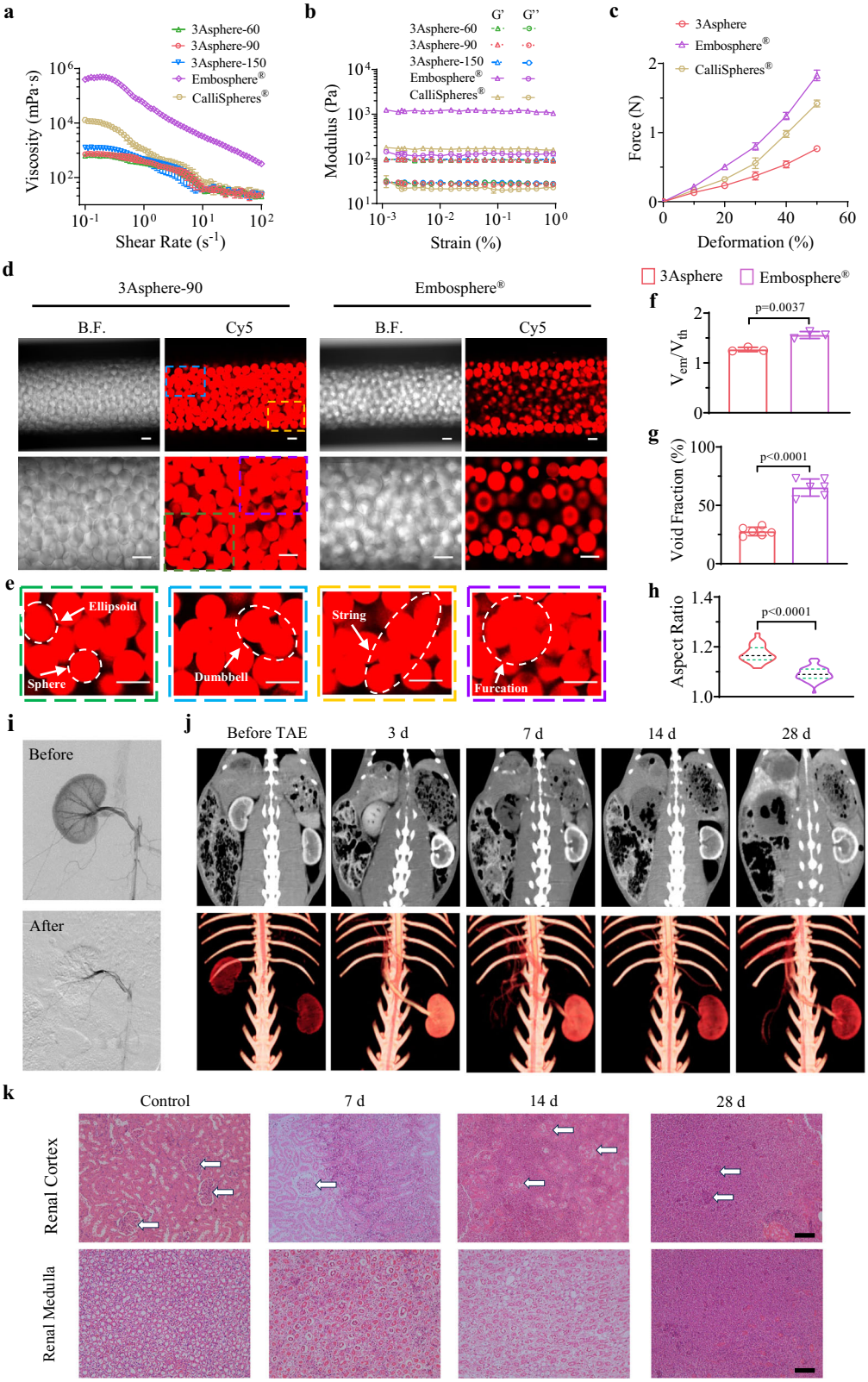

was distributed in the vessels with diameters close to those of the microspheres (40–120 μm). The immunohistochemical analysis demonstrated a marked reduction in CD44 staining on tumor vasculature following 6 h embolization with 3Asphere compared to non-embolized controls (Supplementary Fig. 22), indicating specific ligand-receptor interactions between 3Aspheres and CD44-positive endothelial cells within tumor vasculature.

Embolic effects of thrombin-loaded 3Asphere

Thrombin (Th) can generate fibrin via the proteolytic cleavage of fibrinogen to promote the formation of obstructive thrombosis and tumor vascular infarction[28–30]. Here, Th was introduced into 3Asphere to enhance the occlusion of distal and fine tumor vessels (Fig. 6a). Th-loaded 3Asphere (Th-3Asphere) easily fabricated by adding thrombin solution to 3Asphere displayed fast and high-level loading with a drug

Fig. 3 | Mechanical properties and embolization effect of 3Asphere. a Viscosity of 3Asphere, Embosphere®, and CalliSpheres® by shear rate sweeps ($n = 3$ biological samples). **b** Storage modulus (G′) and loss modulus (G″) as characterized by oscillatory strain sweeps ($n = 3$ biological samples). **c** Compression force-strain curves ($n = 3$ biological samples). **d** Embolization effect of 3Asphere-90 and Embosphere® in capillary glass tubes observed using CLSM ($n = 3$ independent experiments). Scale bars: 100 μm. **e** Amplification of embolization zones in 3Asphere-90 group, showing the elastic deformation of one, two, and multiple 3Asphere in the process of embolization ($n = 3$ independent experiments). Scale bars: 100 μm. **f** Ratios of the embolized volume (V_{em}) in capillary glass tubes to the theoretical volume (V_{th}) of total 3Asphere or Embosphere® ($n = 3$ biological samples). V_{em} was the cross-sectional area multiplied by the embolized height of capillary tubes and V_{th} was the microsphere number multiplied by the volume of one microsphere. **g** Void fraction of the capillary tubes embolized with 3Asphere and Embosphere® ($n = 6$ biological samples). **h** Aspect ratios of 3Asphere and Embosphere® in the capillary tubes ($n = 50$ samples). **i** Representative digital subtraction angiography (DSA) of the right 3Asphere-embolized kidney of rabbits. **j** Representative computed tomography angiography (CTA) images of the right (embolization) and left (control) kidneys of rabbits on days 3, 7, 14, and 28. **k** Representative histopathologic images of right kidney following 3Asphere embolization for 7, 14, and 28 days ($n = 3$ independent experiments). White arrow indicated the glomeruli, and the control group was the unembolized left kidney. Scale bars: 100 μm. Data are presented as mean ± SD. Statistical analysis was performed using unpaired two-tailed Student's t-test. Source data are provided as a Source Data file.

loading efficiency (DLE) of approximately 90% when the theoretical drug loading content (DLC) ranged from 2.5 to 7.5 wt.% (Fig. 6b, Supplementary Fig. 23a). Th loading caused little change in size distribution, viscosity, or modulus of microspheres (Supplementary Fig. 23b, c, Fig. 24). Besides, Th-3Asphere presented a sustained release of Th within 120 h in phosphate buffered saline (PBS) (Fig. 6c) and induced fibrin gel formation similar to free Th (Supplementary Fig. 25) by converting fibrinogen to fibronectin (Supplementary Fig. 26). The addition of Th-3Asphere into anticoagulant whole blood induced obvious blood clots (Fig. 6d), which were stable as indicated by the low absorbance of hemoglobin in the supernatant when the blood clots were dispersed in water (Fig. 6e). Importantly, tumor cells (Hepa1-6 and HepG2) and healthy cells (L929) incubated with Th-3Asphere for 48 h presented more than 95% viability, as indicated by CCK-8 assays (Supplementary Fig. 27). Live/dead staining revealed that nearly all cells incubated with 3Asphere or Th-3Asphere were stained with calcium acetoxymethyl (green fluorescence) (Supplementary Fig. 28), corroborating their good biocompatibility.

Th-3Asphere induced significantly higher levels of tumor growth suppression (Fig. 6f, g) and tumor cell necrosis than 3Asphere (Fig. 6h), as revealed by computed tomography (CT) and MRI on day 14. Notably, Th-3Asphere induced extensive thrombi with significant fibrin clotting in segmental hepatic arteries down to 20 μm (Fig. 6i), whereas no discernible fibrin clots were detected in the 3Asphere group (Supplementary Fig. 29). Moreover, rabbits treated with Th-3Asphere resulted in higher levels of tumor cell necrosis (H&E staining) and apoptosis (terminal deoxynucleotidyl transferase dUTP nick end labeling, TUNEL), and lower levels of cell proliferation (Ki67 staining) and tumor vascularization density (CD31 staining) than those in the 3Asphere group (Fig. 6j–l and Supplementary Fig. 30), corroborating that the introduction of Th promoted obstructive thrombosis and induced vessel infarction. Importantly, Th-3Asphere caused little body weight changes, no detectable damage to major organs, and negligible influence on liver and kidney functions (Supplementary Figs. 31–33). Moreover, the activated partial thromboplastin time (APTT), thrombin time (TT), prothrombin time (PT), and fibrinogen (FIB) level in peripheral blood were not obviously affected by Th-3Asphere (Supplementary Fig. 34), suggesting that the released Th was mainly located in tumor sites and caused little effect on systemic coagulation. Thus, the combination of 3Asphere and thrombin provides a potent strategy to occlude tumor vessels of different sizes, including distal and fine vessels for improved therapeutic outcomes.

EPI-loaded 3Asphere for TACE

3Asphere exhibited fast EPI encapsulation and achieved nearly complete drug loading within 1 min at a theoretical DLC of 30 wt.% (Fig. 7a, Supplementary Movie 2), whereas more than 20 min were required for EPI loading of CalliSpheres®. CLSM revealed that EPI was evenly distributed in 3Asphere (Fig. 7b). At theoretical DLC ranging from 10 to 50 wt.%, 3Asphere displayed quantitative loading with EPI concentrations up to 100 mg/mL (Fig. 7c), and little changes in size and size distribution (Supplementary Fig. 35). The loading of EPI was partly reduced by addition of sodium chloride (NaCl) or urea, in which DLE decreased to 70% at 150 mM NaCl (Supplementary Fig. 36), indicating that EPI loading in 3Asphere is predominantly driven by electrostatic and hydrogen-bond interactions. Additionally, EPI-3Asphere exhibited long-term storage stability, displaying negligible size changes and drug leakage at 4 °C over 12 months (Fig. 7d). Given a relatively high HAase concentration and acidic condition in tumor environments[31,32], we investigated the in vitro drug release of EPI-3Asphere in PBS (pH 6.5) containing 50 U/mL HAase. Under these conditions, more than 95% of the encapsulated EPI was released from EPI-3Asphere over 56 days (Fig. 7e). Interestingly, EPI-3Asphere while exhibited substantial drug release (40–60%) within 7 d under HAase exposure had no detectable changes in volume and morphology (Supplementary Fig. 37). The progressive degradation of HA led to obvious microsphere damage after 14 d incubation. To better mimic the condition of human tumor blood vessels, drug release behavior was further examined in PBS (pH 6.5) supplemented with 10% fetal bovine serum (FBS) and HAase. As shown in Supplementary Fig. 38, 3Asphere demonstrated comparable EPI release kinetics to that observed in FBS-free medium. The cumulative EPI release reached approximately 13% at 24 h and 25% at 48 h, indicating that 3Asphere would likely display a sustained drug release without burst release in the tumor blood vessels. In contrast, CalliSpheres® showed approximately 40% drug release at pH 6.5 within 14 days, followed by sluggish release (< 5%) until day 30 (Supplementary Fig. 39). 3Asphere also induced fast and efficient encapsulation (DLE >90%) and sustained release of irinotecan and cisplatin (Supplementary Figs. 40, 41).

3-[4,5-Dimethylthiazol-2-yl]-2,5 diphenyl tetrazolium bromide (MTT) assays showed that the cytotoxicity of EPI-3Asphere to tumor cells (Hepa1-6, SMMC-7721, and HepG2) was comparable to that of free EPI (Supplementary Fig. 42). In VX2 tumor-bearing rabbits, EPI-3Asphere demonstrated significantly better tumor growth suppression than EPI-CalliSpheres® as revealed by CT imaging on days 7 and 14 (Fig. 7f, g). Moreover, rabbits treated with EPI-3Asphere revealed a significantly extended MST of 63 d (Fig. 7h) and little change in body weight (Supplementary Fig. 43). The antimetastatic effect of EPI-3Asphere was assessed by quantifying metastatic nodes in the lungs of VX2-bearing rabbits on day 14 (Fig. 7i). CT images revealed fewer metastatic nodules in the lungs of rabbits in the EPI-3Asphere group than in those of rabbits in the control and EPI-CalliSpheres® groups, which was confirmed by H&E-stained lung tissue sections (Fig. 7j, k). Thus, 3Asphere featuring fast and robust drug loading, sustained drug release, and vessel-adaptable and adhesive embolization might serve as a potent platform for TACE of liver tumors.

Discussion

In this study, covalently crosslinked 3Asphere presented not only high in vitro and in vivo stability during embolization but also decent deformability and a significantly lower viscosity and modulus than commercial Embosphere® (Fig. 3a, b) and lipiodol microspheres

https://doi.org/10.1038/s41467-025-61621-4

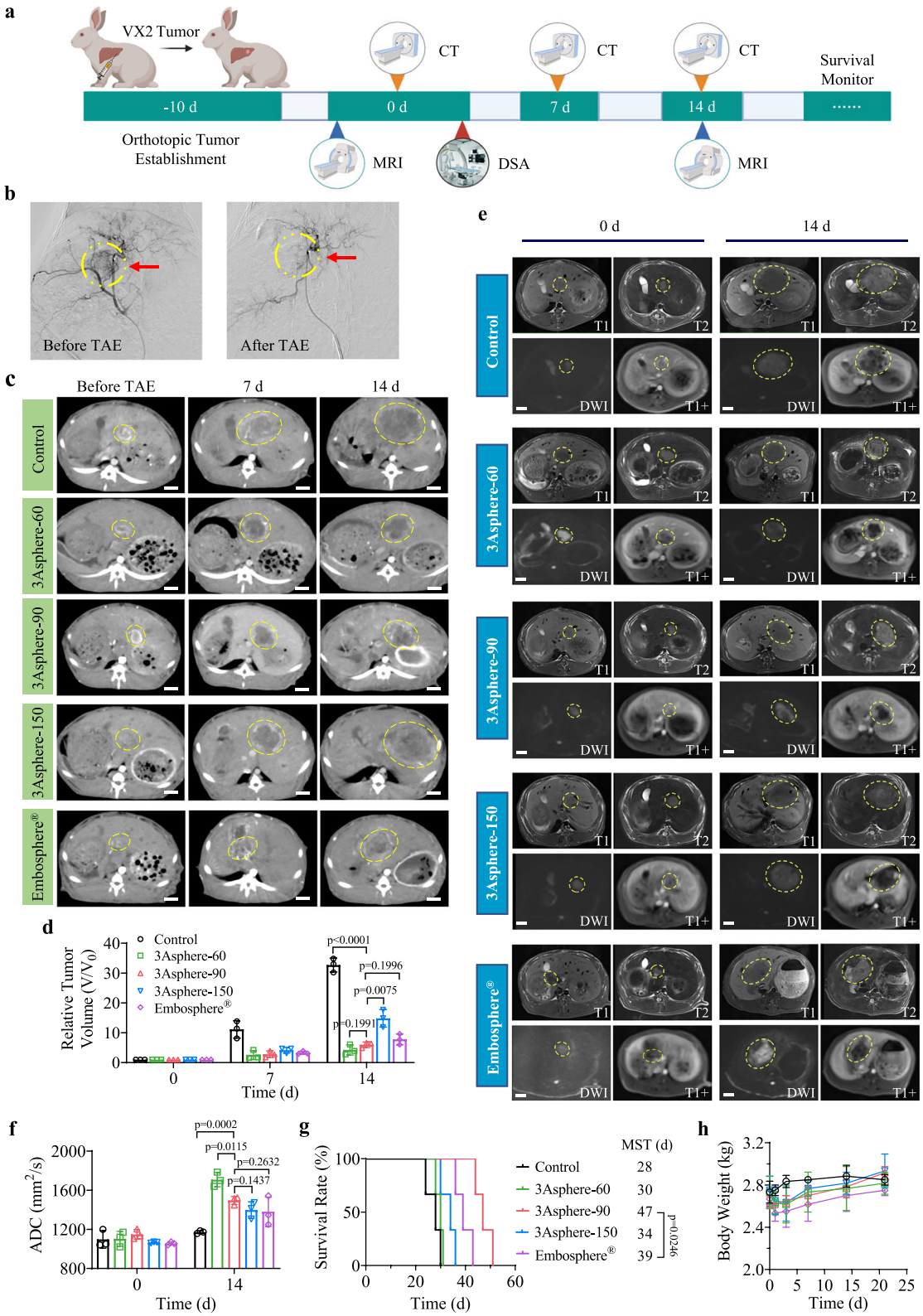

Fig. 4 | Size effect of 3Asphere on transarterial embolization (TAE) therapy in rabbits bearing VX2 tumor. a Schematic diagram of the experimental schedule. Created in BioRender. BioRender.com/kz59339. **b** Representative DSA imaging of tumors before and after TAE using 3Asphere-90. **c** Representative CT-enhanced images. Scale bars: 1 cm. **d** Relative tumor growth volume ($n = 3$ rabbits in each group). Statistical analysis was performed using unpaired two-tailed Student's t-test. **e** Representative magnetic resonance imaging (MRI) of liver (T1: T1 weighted imaging, T2: T2-weighted imaging, DWI: diffusion-weighted imaging, T1+: T1 enhanced imaging). Scale bars: 1 cm. **f** Apparent diffusion coefficient (ADC) ($n = 3$ rabbits in each group). Statistical analysis was performed using unpaired two-tailed Student's t-test. **g** Kaplan-Meier survival curves of tumor-bearing rabbits ($n = 3$ rabbits in each group). Statistical analysis was performed using a log-rank (Mantel-Cox) test. **h** Changes in body weight ($n = 3$ rabbits in each group). Data are presented as mean ± SD. Source data are provided as a Source Data file.

https://doi.org/10.1038/s41467-025-61621-4

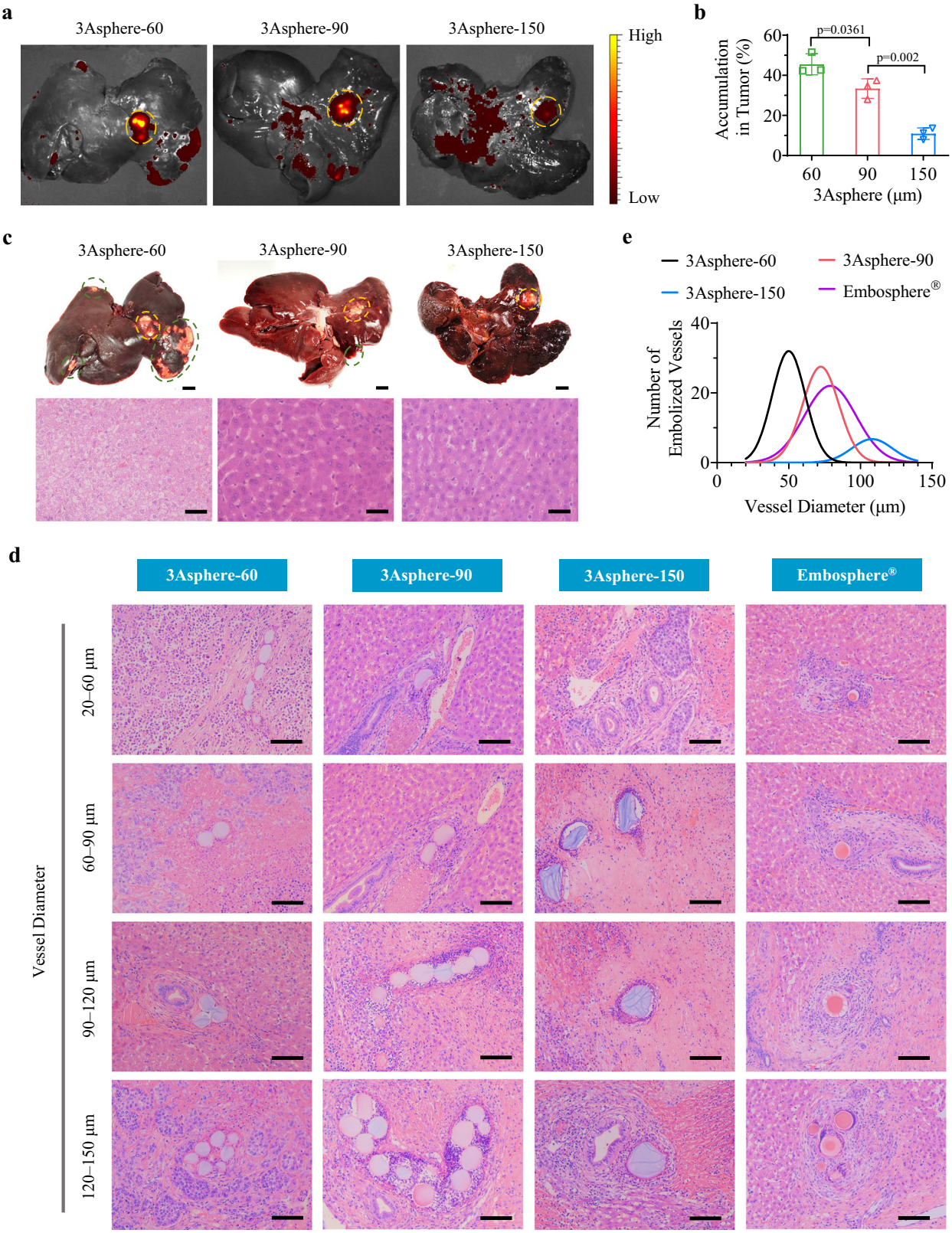

Fig. 5 | 3Asphere distribution in liver, tumor tissue and vessels following the embolization of VX2 tumor in rabbit. a Representative ex vivo images of Cy5-3Asphere in the embolized liver obtained by in vivo imaging system (IVIS) imaging. **b** 3Asphere accumulation in tumor as a percentage of total liver quantified by measuring Cy5 fluorescence of Cy5-3Asphere ($n = 3$ rabbits in each group). Statistical significance was determined using one-way ANOVA with Tukey's post hoc test. **c** Representative gross photos of rabbit livers and H&E staining images of the embolized liver tissue. Yellow circles and green circles refer to the tumor and the necrotic area, respectively. **d** Representative H&E images of vessels with different sizes in tumor sites embolized by 3Asphere (60, 90, 150 μm) and Embosphere® (40–120 μm). **e** Number distribution of embolized vessels with different diameters in tumor tissue according to pathological sections (3Asphere-60, 3Asphere-90, and Embosphere®: $n = 100$ samples; 3Asphere-150: $n = 25$ samples). Scale bars: 1.0 cm (gross photos), 100 μm (H&E images). Data are presented as mean ± SD. Source data are provided as a Source Data file.

https://doi.org/10.1038/s41467-025-61621-4

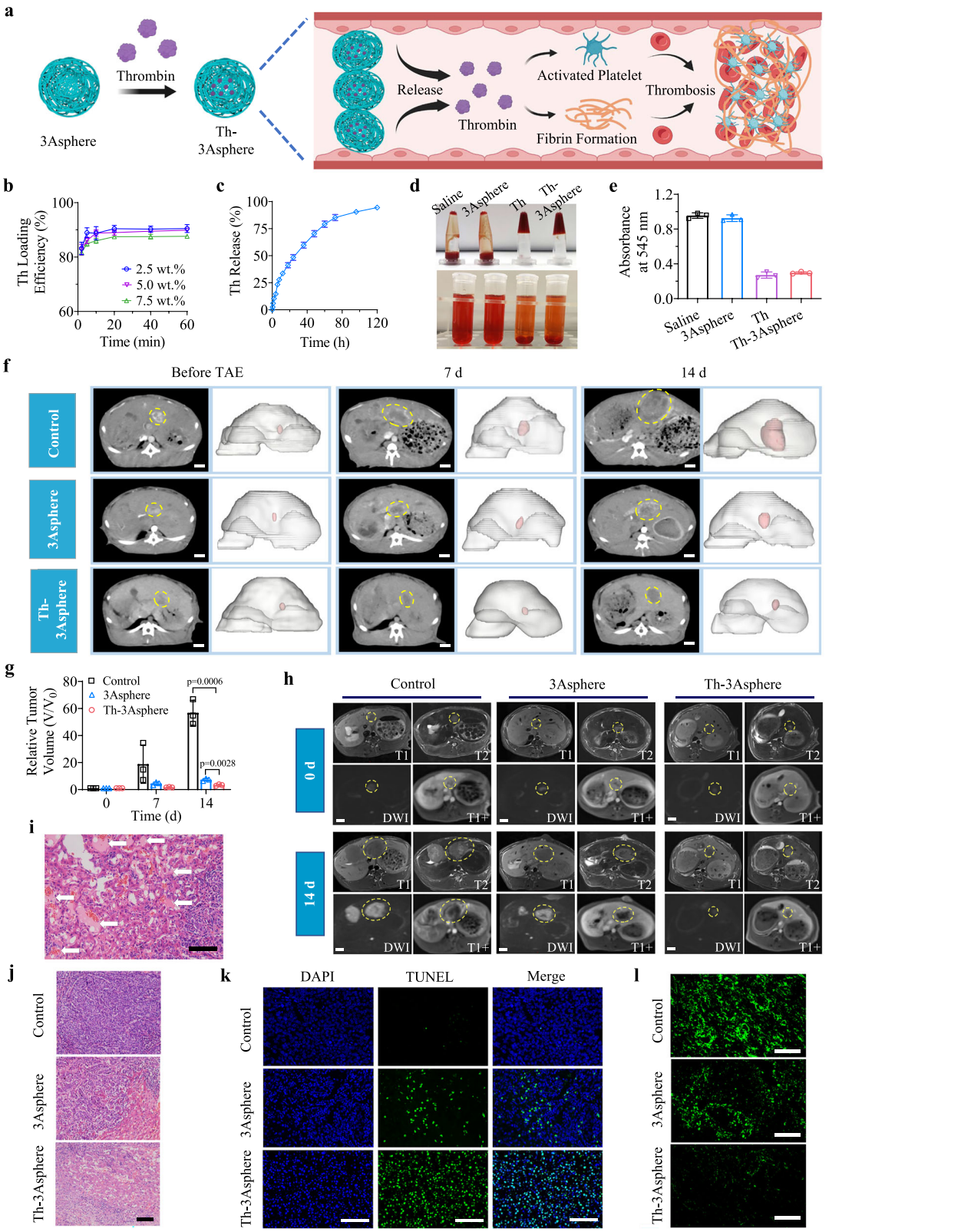

stabilized by Janus particles[11]. In contrast to the broad size distribution of commercial microspheres, 3Asphere fabricated using microfluidics exhibited defined sizes ranging from 50 to 180 μm, which are expected to maximally prevent discontinuous embolization owing to occlusion by large spheres in proximal portions of tumor vessels. In rabbits bearing VX2 tumors, 3Asphere demonstrated an intact structure and vessel-adaptable deformation in tumor vessels following embolization, affording efficient embolization of fine vessels down to 20–60 μm (Fig. 5d). The defined size of 3Asphere allowed exploring the influence of size on biodistribution and embolization, and the results revealed that 3Asphere with smaller sizes accumulated at higher levels in tumor vessels and entered more deeply into distal vessels, resulting in better embolization and tumor suppression. Notably, 3Asphere-60 with the smallest size while showing the best embolization of tumor vessels

Fig. 6 | In vivo embolization effect of thrombin-loaded 3Asphere (Th-3Asphere). a Schematic illustration of embolization and blood coagulation of tumor vessels at the tumor site by Th-3Asphere. Created in BioRender. BioRender.com/d55w789. **b** Thrombin encapsulation in 3Asphere with time at theoretical drug loading contents (DLC) of 2.5–7.5 wt.% ($n = 3$ biological samples). **c** Cumulative Th release from Th-3Asphere in PBS (10 mM, pH 6.5) ($n = 3$ biological samples). **d** Coagulation formation of blood incubated with different groups for 10 min (above photograph), and clots from different groups diluted with 5 mL of water (under photograph) ($n = 3$ independent experiments). **e** Hemoglobin absorbance at 545 nm of supernatants in different groups ($n = 3$ biological samples). **f** Representative CT-enhanced images (left) and 3D reconstruction of CT images (right). Scale bars: 1 cm. **g** Tumor growth with time in different groups ($n = 3$ rabbits in each group). Statistical analysis was performed using unpaired two-tailed Student's t-test. **h** Representative MRI imaging on days 0 and 14. Scale bars: 1 cm. **i** Representative H&E staining to assess thrombosis in tumors treated with Th-3Asphere ($n = 3$ independent experiments). White arrows represent blood clots. Scale bar: 100 μm. **j** Representative H&E staining of tumor sections collected from the tumor-bearing rabbit 14 days after embolization ($n = 3$ independent experiments). Scale bar: 100 μm. **k, l** Representative fluorescent micrographs of TUNEL (**k**) and CD31 (**l**) stained tumor sections collected from a tumor-bearing rabbit at day 14 after TAE treatment ($n = 3$ independent experiments). Scale bars, 100 μm. Data are presented as mean ± SD. Source data are provided as a Source Data file.

extended survival only to a medium level, mainly due to the inevitable occlusion of normal distal arteries in the liver following injection in the PHA of rabbits. The adverse distribution of small 3Asphere in the healthy livers may be avoidable in patients, considering that the injection catheter can directly reach the tumor-feeding arteries rather than the PHA.

In addition to being mechanically adaptable to the tumor blood vasculature, 3Asphere formed from HA derivatives holds the potential to actively bind to tumor vessels via HA-CD44 axis. CD44 is reportedly overexpressed on the endothelial cells of tumor vessels[33,34], and CD44-HA interactions have been exploited to construct HA macroscaffolds and nanosystems for the growth and active drug delivery of CD44-positive cells, respectively[35–38]. 3Asphere displayed active binding to CD44-positive HUVEC and Hepa1-6 HCC cells, whereas commercial Embosphere® showed only few interactions (Fig. 2j). Blocking of CD44 on endothelial cells might also inhibit their proliferation and migration as well as pathological angiogenesis and tumor aggressiveness[39,40].

The occlusion of distal and fine tumor vessels greatly benefits the therapeutic efficacy of embolization. Tumor vessel destruction by disrupting agents or blood clot formation is an attractive modality for cancer therapy[41–44]. However, the nonspecific delivery of disrupting agents and procoagulants often results in moderate therapeutic efficacy and severe damage to normal organs[45]. Compared with 3Asphere, Th-3Asphere induced extensive thrombi with significant fibrin clotting in tumor arteries of sizes down to 20 μm (Fig. 6g), reducing tumor vascular density, increasing the levels of tumor cell necrosis and apoptosis, and significantly enhancing tumor growth suppression. Importantly, the levels of coagulation indicators (APTT, TT, PT, and FIB) in peripheral blood were not obviously affected by Th-3Asphere (Supplementary Fig. 34), suggesting that the released Th was mainly located in tumor sites and caused little effect on systemic coagulation. Therefore, a rational combination of embolization therapy and tumor vascular infarct-inducing drugs, exploiting their respective inherent advantages, holds great promise for achieving potent occlusion of tumor vasculature of different sizes.

Embolic microspheres, mostly based on poly(vinyl alcohol) or poly(methylacrylic acid) are nondegradable, often induce inflammation and foreign body reaction, and hinder reembolization to prevent tumor recurrence[46,47]. Degradable microspheres have been developed using starch or poly(lactic-co-glycolic acid) (PLGA) to block tumor blood-supplying arteries within weeks to months. For example, starch microspheres (DSM, EmboCept®, and Spherex®) composed of crosslinked hydrolyzed starch provide a degradation half-life of 25–60 min, afford transient occlusion to reduce blood flow, and increase the retention of chemotherapeutics in tumors in patients who require multiple treatments and have decreased hepatic function[48,49]. However, DSM is currently available in only one size (~50 μm), does not cause tumor ischemic necrosis as an embolic agent due to its rapid degradation, and is unsuitable for most patients. With an extended degradation time of 12–24 weeks, microspheres formed from PLGA (150–212 μm, Occlusin® 500, IMBiotechnologies Ltd) have been approved for the treatment of unresectable/inoperable hypervascularized tumors[50]. However, the acidic degradation products of PLGA inevitably cause an inflammatory response and fibrous connective tissue production, and long-term clinical benefits have not been demonstrated. 3Asphere exhibited a progressive degradation pattern with approximately 17% degradation in 7 days and more than 90% degradation in 2 months following subcutaneous implantation in rats (Supplementary Fig. 7). In addition, the inflammation and foreign body reaction caused by 3Asphere tended to vanish within 2 weeks. The biodegradability of 3Asphere would improve patient comfort, mitigate the foreign body response, and facilitate repeated embolization. Notably, 3Asphere induced complete embolization of renal arteries for up to 4 weeks and massive ischemic necrosis of the kidney without evidence of recanalization.

TACE has been widely used in the clinical treatment of unresectable HCC; however, embolic microspheres still exhibit slow and insufficient drug loading, and an initial burst release and subsequent trivial, incomplete drug release. For EPI, the most commonly used chemotherapeutic agent in TACE therapy, 3Asphere demonstrates rapid loading (<1 min), a high loading capacity (DLE >99%), a high drug concentration of up to 100 mg/mL, and sustained and nearly complete (>95%) drug release within 56 days. In contrast, CalliSpheres® require up to half an hour for EPI loading before operation and present fast release in the first week, followed by approximately 5% drug release over the next 3 weeks (Supplementary Fig. 39). Moreover, 3Asphere affords efficient encapsulation (DLE >90%) and sustained release of irinotecan and cisplatin, signifying the potent and versatile drug delivery of 3Asphere. Following in vivo TACE treatments, EPI-3Asphere effectively inhibits tumor growth and metastasis and prolongs survival (Fig. 7f–k).

In conclusion, we demonstrated a unique design of tumor vessel-adaptable, adhesive, absorbable microspheres (3Asphere) using microfluidics for sustainable TACE therapy. 3Asphere holds uniform sizes (CV < 2%), high viscoelasticity, and can bind to endothelial cells of tumor vessels to achieve effective blockade of blood supply to the orthotopic VX2 tumor in rabbits, affording effective inhibition of tumor growth and significant survival benefits compared with commercial Embosphere®. In addition, 3Asphere shows fast encapsulation and sustained release of various chemotherapeutics, and TACE with EPI-3Asphere further enhances tumor inhibition and prevents lung metastasis. 3Asphere featuring superb loading of various drugs, sustained drug release, and active and compact embolization holds tremendous potential for the treatment of vascular-related diseases.

Although our results support our proposition that 3Asphere can significantly improve TACE therapy, it is important to note that the blood vessels in rabbits are considerably smaller than those in humans, making it challenging for microcatheters to directly access the tumor vessels. Thus, the precision of tumor embolization and the minimization of off-target vessel blockade in healthy tissues are compromised. In future studies, larger animal models should be utilized to more accurately assess embolization efficacy, therapeutic potential, and off-target distribution of 3Asphere when administered directly into tumor-feeding arteries. We shall further investigate the combination of TACE with other advanced treatment strategies such as molecular target

https://doi.org/10.1038/s41467-025-61621-4

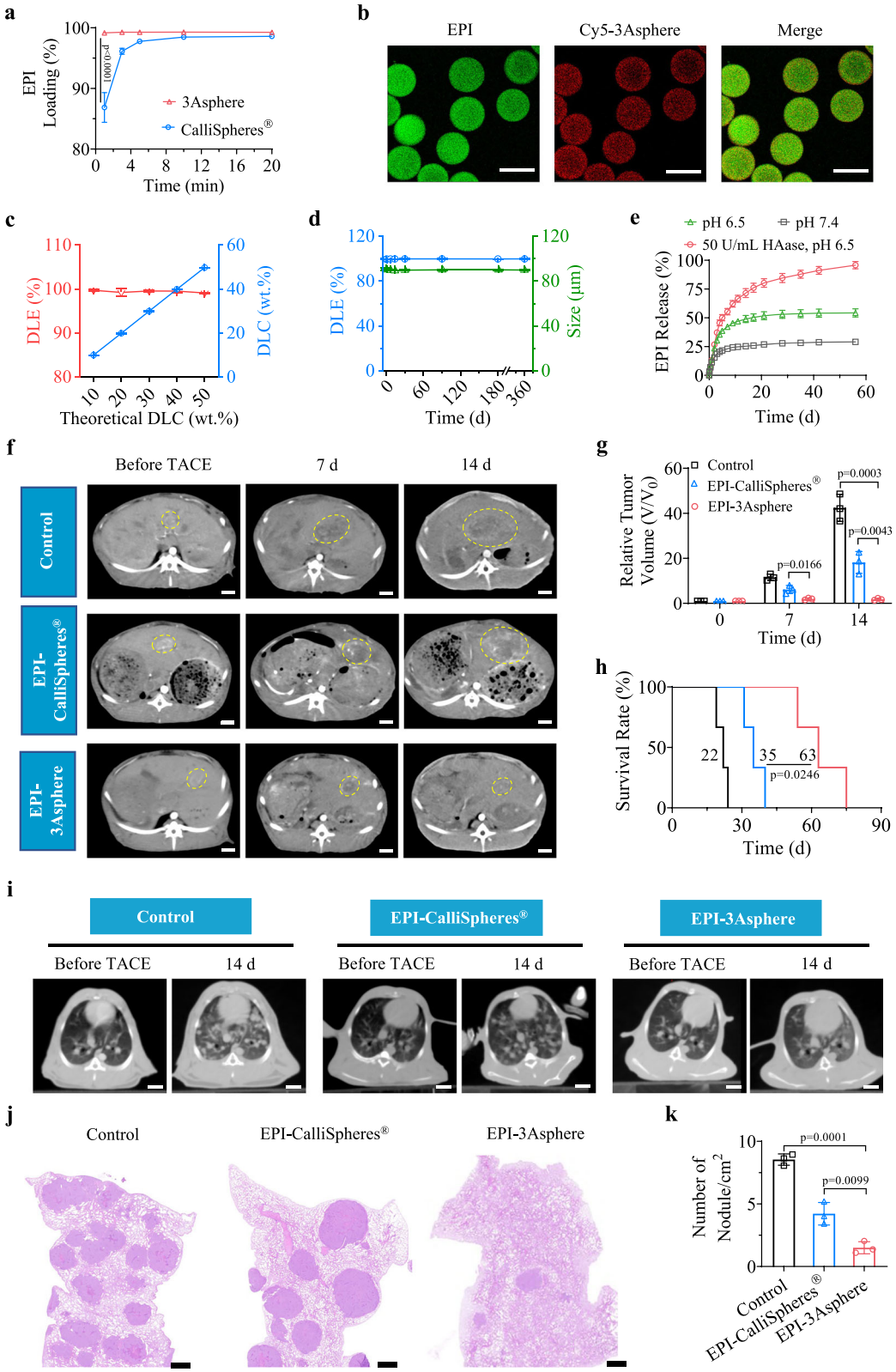

drugs, angiogenesis inhibitors, and immunomodulators for the late stages of hepatocellular carcinoma. Besides hepatocellular carcinoma, 3Asphere also holds significant potential for managing hepatic metastasis from other origins such as pancreatic cancer, colorectal cancer, and neuroendocrine tumors, as well as intrahepatic cholangiocarcinoma currently treated with TACE in clinical practice[51,52].

Methods

Ethical statement

All animal experiments were conducted in accordance with the Guide for the Care and Use of Laboratory Animals and received approval from the Institutional Animal Care and Use Committee of Soochow University (approval number: SUDA20240716A03).

Fig. 7 | Transarterial chemoembolization (TACE) using epirubicin-loaded 3Asphere (EPI-3Asphere). a EPI encapsulation profiles in 3Asphere and CalliSpheres® with time ($n = 3$ biological samples). Statistical analysis was performed using unpaired two-tailed Student's t-test. **b** EPI distribution in 3Asphere observed by CLSM. Cy5-3Asphere: Cy5-labeled 3Asphere ($n = 3$ independent experiments). Scale bars: 100 μm. **c** Drug loading efficiency (DLE) and DLC of EPI at different theoretical DLC ($n = 3$ biological samples). **d** Long-term storage stability of EPI-3Asphere by monitoring the sizes and DLE changes at 4 °C ($n = 3$ biological samples). **e** HAase and pH-dependent EPI release from 3Asphere ($n = 3$ biological samples). **f** Representative CT-enhanced images. Scale bars: 1 cm. **g** Relative tumor growth volume ($n = 3$ rabbits in each group). Statistical analysis was performed using unpaired two-tailed Student's t-test. **h** Kaplan-Meier survival curves of tumor-bearing rabbits ($n = 3$ rabbits in each group). Statistical analysis was performed using a log-rank (Mantel-Cox) test (comparison between EPI-3Asphere and EPI-CalliSpheres®). **i** Representative CT images of tumor metastasis of lung tissues under different treatments. Scale bars: 1 cm. **j** Representative H&E staining slices of lung tissue at 14 days post-treatment ($n = 3$ independent experiments). Scale bars: 2 mm. **k** Tumor metastasis rate per unit area of lung tissues in H&E staining images ($n = 3$ biological samples). Statistical analysis was performed using unpaired two-tailed Student's t-test. Data are presented as mean ± SD. Source data are provided as a Source Data file.

Materials

Sodium hyaluronic acid (HA, molecular weight: 36 kDa) was purchased from Shandong Freda Biopharm Co. Ltd. (Shandong, China). Irgacure 2959 (I2959), mineral oil, Span 80, and thrombin were purchased from Sigma-Aldrich. Sulfo-Cy5-NH_2, sulfo-Cy3-NH_2, and HAase were purchased from Aladdin Chemistry Co., Ltd. (Shanghai, China). CalliSpheres® (Hengrui Pharmaceutical Co., Ltd., China) and Embosphere® (Merit Medical System Inc., USA) were used as received. Cell culture dishes and 96-well plates were purchased from Thermo Fisher Technology Co., Ltd. A Cell Counting Kit-8 (CCK-8, Sigma-Aldrich) and a Micro BCA assay kit (Thermo Scientific) were used according to the manufacturers' instructions. All other reagents and solvents were purchased from Sinopharm Chemical Reagent Co. Ltd. (Shanghai, China) and used as received. Hyaluronic acid-*g*-2-aminoethyl methacrylate (HA-AMA) was synthesized through an amidation reaction between HA and AMA in H_2O/DMSO (v/v, 9/1) at 35 °C using 4-(4,6-Dimethoxy-1,3,5-triazin-2-yl)-4-methylmorpholinium chloride as the coupling agent.

Cell lines and animal study

The L929, HUVEC, HepG2, Hepa1-6, SMMC-7721, and VX2 cell lines were purchased from the Chinese Academy of Sciences (Shanghai) Cell Bank. L929 and HUVEC cells were cultured in 1640 medium containing penicillin (10 U/mL), streptomycin (0.1 mg/mL) and FBS (10%, v/v). HepG2 cells, Hepa1-6, SMMC-7721, and VX2 cells were cultured in high-glucose complete DMEM containing penicillin (10 U/mL), streptomycin (0.1 mg/mL) and FBS (10%, v/v). All the cells were cultured in a 5% CO_2 humidified incubator at 37 °C.

Male Sprague–Dawley (SD) rats (2–3 months, 250–300 g) and New Zealand white rabbits (6–8 months old, 2.5–3.2 kg) were purchased from Beijing Charles River Laboratory Animal Technology Company and Pizhou Dongfang Breeding Co., Ltd, respectively. Findings do not apply to only one sex. In this study design, the sex of the animals was not considered a variable.

Preparation and characterization of 3Asphere

The 3Asphere was fabricated from HA-AMA using microfluidic and free radical polymerization techniques under UV irradiation. In brief, 45 mg/mL of HA-AMA solution in a phosphate buffer (PB, 10 mM, pH 8.5) containing 6.0 mg/mL of I2959 and mineral oil containing 9.0 wt% Span 80 were used as the aqueous and oil phases, respectively. Following the hydrodynamic focus of the aqueous solution with the lateral mineral oil in a microchannel, the microdroplets were formed and irradiated with UV light (365 nm, 30 mW/cm^2) to obtain microspheres, which were purified through sequential washes with isopropyl alcohol, hexane, and PBS. The size and surface morphology of the 3Asphere were assessed using inverted fluorescence microscopy (ECLIPSE Ti, Nikon) and scanning electron microscopy (SEM, SU8010, Hitachi), respectively.

Degradability of 3Asphere

The in vitro degradation behavior was explored using HAase. Typically, 5.0 mg of 3Asphere suspended in HAase solution in PBS (20 U/mL, 50 U/mL, 1.0 mL, pH 7.4) was placed in a shaker (37 °C, 100 rpm). The HAase solution was replaced daily. At predetermined time points, the residual 3Asphere was washed with deionized water, lyophilized, and weighed. The percentage of remaining weight (%) was calculated as follows:

$$Remaining\ weight\ (\%) = \frac{W_t}{W_0} \times 100 \quad (1)$$

Where W_0 was the initial weight of 3Asphere and W_t was the weight of 3Asphere at the predetermined time points. Moreover, the morphological changes of Cy5-labeled 3Asphere were monitored using confocal laser scanning microscopy (CLSM, TCS SP5, Leica).

The in vivo degradability was evaluated by subcutaneously implanting the microspheres (90 μm, 200 μL) into the back of SD rats. At predetermined time points (2, 7, 14, 28, and 56 days), 3Asphere samples were collected for taking pictures and weighing to assess the degradability. Meanwhile, skin tissues surrounding 3Asphere were collected and stained with H&E for histological analysis.

Rheological properties and elasticity of 3Asphere

All rheological measurements were performed using RS6000 rheometer (Thermo Fisher Scientific). For the viscosity test, 0.2 mL of 3Asphere (60, 90, and 150 μm), CalliSpheres® (500–700 μm) or Embosphere® (500–700 μm) was added onto the parallel plate of the rheometer, and the viscosity was measured at 37 °C under different shear rates (0.1–100 s^{-1}). Besides, the storage modulus (G′) and the loss modulus (G″) of different microspheres were similarly measured at 37 °C under different shear strains (10^{-3}–1%).

A texture analyzer (CT-3-1500 g, BrookField) equipped with a cylindrical probe (6.0 mm diameter) and a load cell (5.0 g) was used to evaluate the elasticity of 3Asphere. A monolayer of 3Asphere (580 μm), CalliSpheres® (500–700 μm), or Embosphere® (500–700 μm) was placed in 35 mm petri dish. The initial contact force was set to 0.01 N and the probe was dropped at a rate of 0.01 mm/s until 50% deformation was reached. The morphology of the compressed microspheres was further monitored using inverted microscopy. All tests were performed at least three times.

Embolization in capillary glass tubes

Semiclosed capillary glass tubes with an inner diameter of 0.7 mm were used to imitate embolization. Briefly, 25 μL of 3Asphere or Embosphere® was injected into the capillary tube using an injection pump at a rate of 0.2 mL/min. The embolization and viscoelastic deformation of 3Asphere in the capillary were observed using CLSM.

Active binding of 3Asphere

Protein G-coated plates (Thermo Fisher Scientific) were first treated with recombinant human CD44 Fc chimeric protein (1.0 μg/mL, BioLegend) at 25 °C for 60 min. Bis(sulfosuccinimidyl)suberate (1.0 mM) was subsequently added and the reaction proceeded for 30 min to attain covalent crosslinking. Then, Cy3-labeled microspheres (3Asphere and Embosphere®) were added to the wells (50 microspheres per well), and the mixture was incubated for an additional

30 min. After washing, the microspheres were photographed and quantified using inverted fluorescence microscopy.

The CD44 expression levels in HUVEC, Hepa1-6, and L929 cell lines were conducted using flow cytometry. Briefly, to 1×10^5 cells resuspended in 100 μL of PBS was added 50 μL of PE anti-mouse/human CD44 (clone IM7, Elabscience Biotechnology Co., Ltd., 1:200 dilution, E-AB-F1100UD). After incubation in darkness at 4 °C for 30 min, the cells were washed with PBS and analyzed using a flow cytometer (FACS Verse, BD Biosciences). Data analysis was performed using FlowJo software (v.10.8.1). In the gating strategy, cells were initially sorted based on forward scatter area (FSC-A) against side scatter area (SSC-A) (Supplementary Fig. 44). Subsequently, adherent cells were excluded using the gating of FSC-A versus FSC height (FSC-H). Finally, the cell population was sorted for CD44-positive cells and the data were presented as histograms.

The active binding of 3Asphere to CD44-positive Hepa1-6 and HUVEC was also assessed. The cells were cultured in 48-well plates (5×10^4 cells, 290 μL per well). After 12 h, one hundred Cy3-labeled microspheres (3Asphere or Embosphere®) in 10 μL of PBS were added and incubated at 37 °C for 4 h. Following two washes with PBS, the cells were fixed and stained with DAPI. Finally, the cells and microspheres were photographed with inverted fluorescence microscopy, and the number of microspheres per well was counted.

In vitro drug loading and release

0.3 mL of 3Asphere (10 mg/mL) was incubated with an equivalent volume of thrombin solution at different concentrations. At predetermined time points (2, 5, 10, 20, 40, and 60 min), 20 μL of the supernatant was taken, and the unloaded thrombin was quantified using Micro BCA. The amount of loaded thrombin was determined by subtracting the unloaded thrombin from the total amount of fed thrombin. The drug loading efficiency (DLE) and drug loading content (DLC) were calculated according to the following formulas:

$$\mathrm{DLC(wt.\%)} = \frac{\text{Weight of loaded drug}}{\text{Weight of 3Asphere + loaded drug}} \times 100 \quad (2)$$

$$\mathrm{DLE(\%)} = \frac{\text{Weight of loaded drug}}{\text{Weight of fed drug}} \times 100 \quad (3)$$

In vitro thrombin release was performed using a transwell system (pore size: 8.0 μm, Corning, cat. No. 3422). 300 μL of Th-3Asphere (500 μg thrombin) were loaded into the upper chamber, which was immersed in the release medium (PBS 7.4 or 6.5). The released thrombin collected from the bottom of the chamber at different time points was measured using Micro BCA kit.

The in vitro loading of chemotherapeutics like EPI, irinotecan, and cisplatin was similarly performed. For monitoring the encapsulation profiles of 3Asphere with time, the drugs in the supernatant were collected at a series of time points. The amount of EPI, irinotecan, and cisplatin (following the reaction with 1,2-Diaminobenzene) was quantified using UV spectrophotometer (UH5300, Hitachi) to acquire drug loading level within 3Asphere. To investigate the EPI loading mechanism in 3Asphere, the loading capacity was examined in media containing NaCl or urea. 3Asphere suspension underwent three sequential washing cycles with NaCl or urea solutions at predetermined concentrations. Then, 0.3 mL of EPI solution (4.3 mg/mL) was combined with an equal volume of the treated 3Asphere suspension. After mixing for 5 min, the unencapsulated EPI in the supernatant was quantified using UV spectrophotometer to determine the drug loading efficiency.

In vitro drug release was carried out in release media including (i) PBS (150 mM, pH 7.4), (ii) PBS (150 mM, pH 6.5), (iii) PBS (150 mM, pH 6.5) containing HAase (50 U/mL), (iv) PBS (150 mM, pH 6.5) containing 10% FBS, and (v) PBS (150 mM, pH 6.5) containing 10% FBS and 50 U/mL of HAase. The morphological changes of EPI-3Asphere during drug release were observed using inverted fluorescence microscopy.

In vitro procoagulant property of Th-3Asphere

To assess the procoagulant ability of thrombin after the encapsulation of 3Asphere, free thrombin and Th-3Asphere with equal amount of thrombin (10 U/mL) were mixed with the fibrinogen solution (10 mg/mL). After incubation at 37 °C for 10 min, the transmittance of the solutions was measured using UV spectrophotometer. In addition, the formation of fibrin from FITC-labeled fibrinogen in the solution was observed using inverted fluorescence microscopy.

Rabbit blood was used to assess the potency of the blood clotting formation by Th-3Asphere. 250 μL of thrombin or Th-3Asphere at a thrombin concentration of 10 U/mL was added to equivalent volume of whole blood from rabbit. After incubation at 37 °C for 10 min, photographs of the coagulation in each group were taken. Then, 5.0 mL of deionized water was added to each group to lyse the non-clotted red blood cells, and the absorbance of the supernatant was measured at 545 nm using a UV spectrophotometer.

Cell and blood compatibility of 3Asphere

The cytotoxicity of 3Asphere was studied by a CCK-8 assay. L929, SMMC-7721, HepG2, Hepa1-6, and VX2 cells were cultured in 96-well plates (3×10^3 cells, 90 μL per well) for 12 h at 37 °C. Then, 3Asphere (90 μm, 10 μL) at different concentrations was added, and the cells were incubated at 37 °C for 48 h. 10 μL of CCK-8 solution was added to each well and incubated for 2 h. The absorbance of all the samples were measured using a microplate reader at 450 nm.

A live/dead staining assay was used to evaluate the viability of cells treated with microspheres. Hepa1-6 and HepG2 cells were added to 24-well plates at a density of 2×10^4 cells per well and cultured for 12 h at 37 °C. Then, 200 μg/mL of 3Asphere with different thrombin concentrations were added, and the cells were incubated for 48 h at 37 °C. The cells were stained with a calcein-AM/PI cell viability/cytotoxicity kit for live/dead assay.

The hemolysis of 3Asphere was evaluated using rabbit blood, which was collected from healthy rabbits. The upper plasma was removed by centrifugation (500 × *g*, 4 °C, 10 min), and the residual cells were washed with 0.9% NaCl solution until the supernatant was colorless. Then, the red blood cells in 0.9% NaCl solution were mixed with 3Asphere at a concentration of 200 or 1000 μg/mL and incubated at 37 °C for 20 min. The absorbance of the supernatant was measured by a UV spectrophotometer at 545 nm. 0.9% NaCl saline and deionized water were used as the negative and positive controls, respectively. OD_s, OD_n, and OD_p represent the ultraviolet absorbance of the samples, negative and positive controls, respectively. The hemolysis rate (HR%) was calculated by the following formula:

$$\mathrm{HR(\%)} = \frac{OD_s - OD_n}{OD_p - OD_n} \times 100 \quad (4)$$

Cytotoxicity of EPI-3Asphere

The cytotoxicity of EPI-3Asphere on HCC cells (Hepa1-6, SMMC-7721, and HepG2) was assessed using MTT assay. Hepa1-6, SMMC-7721, and HepG2 cells (3×10^3 cells/well) were seeded into 96-well plates and incubated for 12 h. EPI or EPI-3Asphere (20 μL) was then added, and the cells were incubated at 37 °C for 48 h. Following the incubation with MTT (5 mg/mL, 10 μL) for 4 h, the formed formazan crystals were dissolved in DMSO and measured using a microplate reader at the absorbance of 570 nm. The cell viability was calculated by comparing the absorbance of the treated groups to that of PBS group.

Renal embolization evaluation of 3Asphere

To investigate the embolization behavior of 3Asphere in renal arteries, New Zealand rabbits were intramuscularly injected with telazol (0.2 mL/kg) for anesthesia after fasting for 12 h. The rabbits were then positioned supine on the animal operating table (Supplementary Fig. 45a). Afterward, the femoral artery was exposed in the groin, and a microcatheter was introduced into the femoral artery (Supplementary Fig. 45b, c). Under the guidance of X-ray fluoroscopy (digital subtraction angiography, DSA, Siemens Bicor Top., Germany), 3.0 mL of iodixanol was injected to visualize the distribution of the abdominal vasculature. Subsequently, the catheter was slowly introduced into the right renal artery under DSA, and angiography was performed again to determine the renal arterial distribution. Then, 1.0 mL of a mixture of 3Asphere-90 and iodixanol (1:1, v/v) was injected into the renal arteries at a rate of 1.0 mL/min. After the embolization of the renal artery, angiography was performed again to confirm the renal embolization outcome. Finally, the microcatheter was slowly removed, and the wound was sutured and disinfected (Supplementary Fig. 45d), followed by intramuscular injection of antibiotics for 3 days to prevent infection.

On days 3, 7, 14, and 28 after renal artery embolization, contrast-enhanced computed tomography was performed by injecting contrast agents (iodixanol, 3 mL) to assess the embolization effect. Moreover, one rabbit was euthanized, and both kidneys were fixed in 4.0% paraformaldehyde solution for H&E staining analysis.

In vivo embolization of liver tumors

An orthotopic liver cancer model was established by transplanting VX2 tumor tissues into the left liver lobe of rabbits with the assistance of CT imaging. After ten days, the VX2 tumor-bearing rabbits (maximum tumor diameter: 0.8–1.3 cm) were randomly divided into five groups ($n = 3$) and treated the following formulations: (i) control; (ii) 3Asphere-60; (iii) 3Asphere-90; (iv) 3Asphere-150; and (v) Embosphere® (40–120 μm). Under DSA guidance, a 2.4-F microcatheter (Progreat, Terumo Co., Tokyo, Japan) was introduced into the PHA of the rabbits. Angiography was then performed to visualize the distribution of the hepatic arteries and the location of the hepatic tumor. Afterward, 0.2 mL of the mixture of microspheres and iodixanol (3:7, v/v) was slowly injected into the hepatic artery via a microcatheter, and the vessel occlusion was confirmed by DSA imaging. The tumor volumes were determined by contrast-enhanced CT scanning with iodixanol injection on days 7 and 14, and 3.0 T magnetic resonance imaging (MRI, Magnetom Skyra scanner (Siemens Healthcare GmbH, Erlangen, Germany)) on day 14. In MRI imaging, axial T1-weighted imaging (T1WI), T2-weighted imaging (T2WI), diffusion-weighted imaging (DWI), and Gd-DTPA enhanced T1WI (T1 +) sequence scans were included. The tumor volume was estimated by its largest (a) and smallest (b) diameters using the following formula:

$$\text{Tumor volume}\,(\text{cm}^3) = \frac{a \times b^2}{2} \quad (5)$$

In addition, the blood of the rabbits (1.0 mL per rabbit) was collected in procoagulant tubes at various time points (before and 1, 3, and 7 days after embolization) and centrifuged (4 °C, 3000 rpm, 5 min) to obtain the serum. Afterward, the values of ALT, AST, ALB, TBIL, BUN, and CREA were determined by biochemical analyzer to evaluate the liver and kidney function.

For the in vivo embolization of Th-3Asphere, the VX2 tumor-bearing rabbits were randomly divided into three groups (n = 3): (i) control; (ii) 3Asphere-90 (200 μL); and (iii) Th-3Asphere-90 (200 μL, Th: 100 U per rabbit). After TAE treatment, the tumor growth was similarly evaluated by CT and MRI. In addition, the coagulation function indices (APTT, TT, PT, and FIB) were determined at 14 days after embolization. To evaluate the TACE effect of EPI-3Asphere, the VX2 tumor-bearing rabbits were randomly divided into three groups ($n = 3$): (i) control; (ii) EPI-CalliSpheres® (100–300 μm, 200 μL); and (iii) EPI-3Asphere (90 μm, 200 μL). After TACE treatment, the tumor growth and lung metastasis were evaluated by CT imaging. The body weight of the rabbits was monitored every three days. When the body weight loss exceeded 15%, the rabbits were humanely euthanized.

Evaluation of histopathology and immunofluorescence

For the analysis of rabbit tissue sections, tumors and major organs were collected, fixed in 4% paraformaldehyde overnight, sectioned, and stained according to the kit instructions. H&E-stained sections were observed under an inverted fluorescence microscope, while TUNEL and immunofluorescence-stained sections (Ki67 and CD31) were observed by CLSM. Immunofluorescence images were analyzed using K-viewer (v 1.7.1).

Liver distribution of 3Asphere

To characterize the distribution of 3Asphere with different sizes in the liver, rabbits bearing orthotopic VX2 tumors were divided into three groups for embolization (n = 3): (i) Cy5-labeled 3Asphere-60; (ii) Cy5-labeled 3Asphere-90; and (iii) Cy5-labeled 3Asphere-150. After embolization for 3 days, the liver tissues were harvested to observe the distribution of 3Asphere using a near-infrared fluorescence imaging system (IVIS Lumina II, Ex. 620 nm and Em. 670 nm). Then, the tumor and liver tissues were separately fixed in a 4% paraformaldehyde solution for H&E staining to analyze the distribution of the microspheres. To evaluate the binding efficacy of 3Asphere to CD44 on tumor vessels, VX2 tumor-bearing rabbits were sacrificed 6 h post-embolization with 3Asphere. The resected tumors were fixed and sectioned for immunofluorescence staining analysis of CD31 and CD44.

Statistical analysis

The results of this work are presented as the means ± standard deviations (SD). Statistical analysis was performed with GraphPad Prism software 8. One-way analysis of variance (ANOVA) with Tukey's multiple comparisons and an unpaired two-tailed Student's t-test were used to establish the significant differences among groups. The survival rate was analyzed by the Kaplan-Meier method with a log-rank (Mantel-Cox) test. Statistical significance was defined as $^{*}p < 0.05$, $^{**}p < 0.01$, $^{***}p < 0.001$, and $^{****}p < 0.0001$.

Data availability

The main data in this study are provided in the paper, supplementary information, and source data files. All other data are available from the corresponding author. Source data are provided with this paper.

References

1. Forner, A., Gilabert, M., Bruix, J. & Raoul, J. L. Treatment of intermediate-stage hepatocellular carcinoma. *Nat. Rev. Clin. Oncol.* **11**, 525–535 (2014).
2. Llovet, J. M. et al. Locoregional therapies in the era of molecular and immune treatments for hepatocellular carcinoma. *Nat. Rev. Gastroenterol. Hepatol.* **18**, 293–313 (2021).
3. Reig, M. et al. BCLC strategy for prognosis prediction and treatment recommendation: The 2022 update. *J. Hepatol.* **76**, 681–693 (2022).
4. Mikhail, A. S. et al. Drug-eluting embolic microspheres: State-of-the-art and emerging clinical applications. *Expert Opin. Drug Deliv.* **18**, 383–398 (2021).
5. Pérez-López, A., Martín-Sabroso, C., Gómez-Lázaro, L., Torres-Suárez, A. I. & Aparicio-Blanco, J. Embolization therapy with microspheres for the treatment of liver cancer: State-of-the-art of clinical translation. *Acta Biomater.* **149**, 1–15 (2022).
6. Hu, J. et al. Advances in biomaterials and technologies for vascular embolization. *Adv. Mater.* **31**, e1901071 (2019).

7. Jia, G. et al. Recent advances and applications of microspheres and nanoparticles in transarterial chemoembolization for hepatocellular carcinoma. *Wiley Interdiscip. Rev. Nanomed. Nanobiotechnol.* **14**, e1749 (2022).
8. Liu, M. H. et al. Solvent exchange induced in situ formed hydrogel as liquid embolic agents. *Adv. Funct. Mater.* **33**, 2305153 (2023).
9. Sakr, O. S. et al. Explosomes: A new modality for DEB-TACE local delivery of sorafenib: In vivo proof of sustained release. *J. Control. Release* **364**, 12–22 (2023).
10. Chen, P., Varghese, P. J. G., Zhao, K. R. & Hu, J. J. Mechanical investigation of a Tandem embolization-visualization system for minimally invasive procedures. *J. Mech. Behav. Biomed. Mater.* **160**, 106739 (2024).
11. Tao, S. J. et al. Janus particle-engineered structural lipiodol droplets for arterial embolization. *Nat. Commun.* **14**, 5575 (2023).
12. Li, J. et al. Fusible and radiopaque microspheres for embolization. *Adv. Mater.* **36**, 2405224 (2024).
13. Ma, Y. T. et al. Biodegradable microembolics with nanografted polyanions enable high-efficiency drug loading and sustained deep-tumor drug penetration for locoregional chemoembolization treatment. *ACS Nano* **18**, 18211–18229 (2024).
14. Choi, H. J. et al. On-demand degradable embolic microspheres for immediate restoration of blood flow during image-guided embolization procedures. *Biomaterials* **265**, 120408 (2021).
15. Zheng, Z. Y. et al. Idarubicin-loaded biodegradable microspheres enhance sensitivity to anti-PD1 immunotherapy in transcatheter arterial chemoembolization of hepatocellular carcinoma. *Acta Biomater.* **157**, 337–351 (2023).
16. Zheng, D.-W. et al. Biomaterial-mediated modulation of oral microbiota synergizes with PD-1 blockade in mice with oral squamous cell carcinoma. *Nat. Biomed. Eng.* **6**, 32–43 (2022).
17. Zhu, Y. J. et al. Metallo-alginate hydrogel can potentiate microwave tumor ablation for synergistic cancer treatment. *Sci. Adv.* **8**, eabo5285 (2022).
18. Xian, J. et al. Elemene hydrogel modulates the tumor immune microenvironment for enhanced treatment of postoperative cancer recurrence and metastases. *J. Am. Chem. Soc.* **146**, 35252–35263 (2024).
19. Nam, J. et al. Engineered polysaccharides for controlling innate and adaptive immune responses. *Nat. Rev. Bioeng.* **2**, 733–751 (2024).
20. Cao, X. et al. Ternary inulin hydrogel with long-term intestinal retention for simultaneously reversing IBD and its fibrotic complication. *Nat. Commun.* **15**, 8428 (2024).
21. Moragues, T. et al. Droplet-based microfluidics. *Nat. Rev. Methods Prim.* **3**, 32 (2023).
22. Wei, Z. et al. Polymeric microspheres with high mass fraction of therapeutics enabled by the manipulation of kinetics factor during emulsion droplet solidification. *Adv. Funct. Mater.* **35**, 2417307 (2025).
23. Mackman, N., Bergmeier, W., Stouffer, G. A. & Weitz, J. I. Therapeutic strategies for thrombosis: new targets and approaches. *Nat. Rev. Drug Discov.* **19**, 333–352 (2020).
24. Dong, Z. et al. Procoagulant $CaCO_3$-embedded embolic microspheres can potentiate transcatheter arterial embolization of hepatocellular carcinoma. *Nano Today* **55**, 102216 (2024).
25. Toole, B. P. Hyaluronan: from extracellular glue to pericellular cue. *Nat. Rev. Cancer* **4**, 528–539 (2004).
26. Ren, H. et al. Injectable, self-healing hydrogel adhesives with firm tissue adhesion and on-demand biodegradation for sutureless wound closure. *Sci. Adv.* **9**, eadh4327 (2023).
27. Boss, M. A. et al. The QIBA Profile for diffusion-weighted MRI: apparent diffusion coefficient as a quantitative imaging biomarker. *Radiology* **313**, e233055 (2024).
28. Li, S. et al. Combination of tumour-infarction therapy and chemotherapy via the co-delivery of doxorubicin and thrombin encapsulated in tumour-targeted nanoparticles. *Nat. Biomed. Eng.* **4**, 732–742 (2020).
29. Saeed, M. et al. From design to clinic: engineered nanobiomaterials for immune normalization therapy of cancer. *Adv. Mater.* **33**, e2008094 (2021).
30. Hahmann, J., Ishaqat, A., Lammers, T. & Herrmann, A. Sonogenetics for monitoring and modulating biomolecular function by ultrasound. *Angew. Chem. -Int. Ed.* **63**, e202317112 (2024).
31. Guan, M. et al. Regulating copper homeostasis of tumor cells to promote cuproptosis for enhancing breast cancer immunotherapy. *Nat. Commun.* **15**, 10060 (2024).
32. Deng, C., Zhang, Q., Guo, J., Zhao, X. & Zhong, Z. Robust and smart polypeptide-based nanomedicines for targeted tumor therapy. *Adv. Drug Deliv. Rev.* **160**, 199–211 (2020).
33. Griffioen, A. W. et al. CD44 is involved in tumor angiogenesis; an activation antigen on human endothelial cells. *Blood* **90**, 1150–1159 (1997).
34. Chen, L. et al. The role of CD44 in pathological angiogenesis. *Faseb J.* **34**, 13125–13139 (2020).
35. Lee, Y. et al. Hyaluronic acid-bilirubin nanomedicine-based combination chemoimmunotherapy. *Nat. Commun.* **14**, 2041–1723 (2023).
36. Hou, G. H. et al. Bimetallic peroxide nanoparticles induce PANoptosis by disrupting ion homeostasis for enhanced immunotherapy. *Sci. Adv.* **10**, eadp7160 (2024).
37. Lee, W. H. et al. Hyaluronic acid nanoparticles as a topical agent for treating psoriasis. *ACS Nano* **16**, 20057–20074 (2022).
38. Huang, K. et al. Small, traceable, endosome-disrupting, and bioresponsive click nanogels fabricated via microfluidics for CD44-targeted cytoplasmic delivery of therapeutic proteins. *ACS Appl. Mater. Interfaces* **11**, 22171–22180 (2019).
39. Kim, G. H. et al. Selective delivery of PLXDC1 small interfering RNA to endothelial cells for anti-angiogenesis tumor therapy using CD44-targeted chitosan nanoparticles for epithelial ovarian cancer. *Drug Deliv.* **25**, 1394–1402 (2018).
40. Wei, Z. et al. Hydrogels with tunable mechanical plasticity regulate endothelial cell outgrowth in vasculogenesis and angiogenesis. *Nat. Commun.* **14**, 8307 (2023).
41. Guelfi, S., Hodivala-Dilke, K. & Bergers, G. Targeting the tumour vasculature: from vessel destruction to promotion. *Nat. Rev. Cancer* **24**, 655–675 (2024).
42. Ma, Z. et al. Selective thrombosis of tumor for enhanced hypoxia-activated prodrug therapy. *Adv. Mater.* **33**, e2104504 (2021).
43. Sun, J. et al. Azide-masked resiquimod activated by hypoxia for selective tumor therapy. *Adv. Mater.* **35**, e2207733 (2023).
44. Li, H. et al. Light-driven self-recruitment of biomimetic semiconducting polymer nanoparticles for precise tumor vascular disruption. *Adv. Mater.* **35**, e2210920 (2023).
45. Yin, J. et al. Thrombin based photothermal-responsive nanoplatform for tumor-specific embolization therapy. *Small* **17**, e2105033 (2021).
46. Doucet, J. et al. Advances in degradable embolic microspheres: a state of the art review. *J. Func. Biomater.* **9**, 14 (2018).
47. Wang, C. Y., Hu, J., Sheth, R. A. & Oklu, R. Emerging embolic agents in endovascular embolization: an overview. *Prog. Biomed. Eng.* **2**, 012003 (2020).
48. Thaarup, I. C., Gummesson, C. & Bjarnsholt, T. Measuring enzymatic degradation of degradable starch microspheres using confocal laser scanning microscopy. *Acta Biomater.* **131**, 464–471 (2021).
49. Rozzanigo, U. et al. Chemoembolization with degradable starch microspheres (DSM-TACE): Expanding indications in HCC multidisciplinary tumor board. *Hepatoma Res.* **9**, 14 (2023).
50. Owen, R. J. et al. A preclinical study of the safety and efficacy of occlusin™ 500 artificial embolization device in sheep. *Cardiovasc. Interv. Radiol.* **35**, 636–644 (2011).

51. Tsilimigras, D. I. et al. Liver metastases. *Nat. Rev. Dis. Prim.* **7**, 27 (2021).
52. Moris, D. et al. Advances in the treatment of intrahepatic cholangiocarcinoma: An overview of the current and future therapeutic landscape for clinicians. *CA Cancer J. Clin.* **73**, 198–222 (2023).

Acknowledgements

This work was financially supported by the National Key R&D Program of China (2021YFB3800900 received by C.D.) and the National Natural Science Foundation of China (52373299 received by C.D., 51973149 received by C.D.).

Author contributions

Z.Z., C.D., X.Z., J.G., and J.H. conceived and designed the study. J.G., J.H., Z.H., D.H., H.T., and Y.W. performed the experiments. J.G., J.H., and Z.H. participated in data analysis. C.D., J.G., and Z.Z. wrote the manuscript. All authors discussed the results and commented on the manuscript.

Competing interests

The authors declare no competing interests.

Additional information

Supplementary information The online version contains supplementary material available at https://doi.org/10.1038/s41467-025-61621-4.

Correspondence and requests for materials should be addressed to Chao Deng, Xiaoli Zhu or Zhiyuan Zhong.

Peer review information *Nature Communications* thanks Guangjun Nie, and the other, anonymous, reviewer for their contribution to the peer review of this work. A peer review file is available.